Structure and Dynamics of Ferro- and Ferri-Cyanide Anions in Water and Heavy Water: an Insight by MD Simulations and 2D IR Spectroscopy.

ARTICLE *in* THE JOURNAL OF PHYSICAL CHEMISTRY B · NOVEMBER 2014

Impact Factor: 3.3 · DOI: 10.1021/jp511391b · Source: PubMed

THE JOURNAL OF PHYSICAL CHEMISTRY B

Article

pubs.acs.org/JPCB

Structure and Dynamics of Ferrocyanide and Ferricyanide Anions in Water and Heavy Water: An Insight by MD Simulations and 2D IR Spectroscopy

Giacomo Prampolini,*[,†] Pengyun Yu,[§] Silvia Pizzanelli,[†] Ivo Cacelli,[‡] Fan Yang,[§] Juan Zhao,[§] and Jianping Wang[§]

[†]Istituto di Chimica dei Composti OrganoMetallici (ICCOM-CNR), National Research Council (CNR), Area della Ricerca, Via G. Moruzzi 1, I-56124 Pisa, Italy

[‡]Dipartimento di Chimica e Chimica Industriale, Università di Pisa, Via Risorgimento 35, I-56126 Pisa, Italy

[§]Beijing National Laboratory for Molecular Sciences, Molecular Reaction Dynamics Laboratory, Institute of Chemistry, The Chinese Academy of Sciences, Beijing, P. R. China 100190

Supporting Information

ABSTRACT: Combined computational and experimental techniques were employed to investigate at the microscopic level the structural and dynamic properties of ferro- and ferricyanide ions in aqueous solution. The characterization of the structural patterns and multiscale dynamics taking place within the first solvation spheres in water and heavy water solvents was first achieved through extensive molecular dynamics simulations, performed with refined force fields, specifically parametrized for the cyanide ions under investigation. The information gained about the solute−solvent interactions is then validated through the successful comparison of computed and measured waiting-time-dependent 2D IR spectra. The vibrational patterns resulting from 2D IR measurements were rationalized in terms of the interaction between the ion and the neighboring water molecules described by simulation. It was found that, within the first solvation sphere, the stronger interactions of the solvent with the ferro species are responsible for a delay in the relaxation dynamics, which becomes more and more evident on longer time scales.

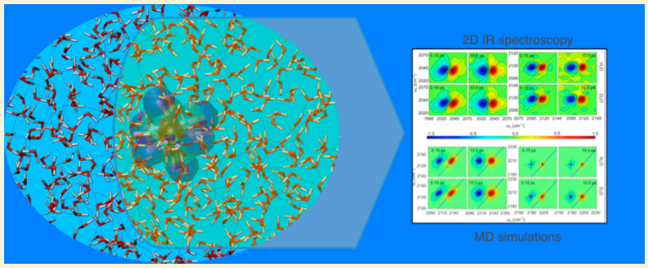

INTRODUCTION

Understanding the behavior of ions in aqueous environment is of fundamental importance in the field of solution-phase chemistry and biochemistry.[1,2] Broadly speaking, water molecules surround the ion, showing rather ordered patterns, which are progressively lost as the distance from the ion increases. However, outer hydration layers may persist through intermolecular hydrogen bonding (HB) interaction. Whether the ionic influence coming from the charged species in the center can go beyond the hydration layers is still under debate.[2] In other words, is such influence localized or delocalized? Initially it was believed that salt ions could be categorized into "water structure breaker (chaotrope)" and "water structure promoter (kosmotrope)", meaning that the ionic influence can extend into the bulk water and is therefore delocalized. Experimental evidence has been found to support this viewpoint.[3,4] However, recent studies[5−10] suggest that the influence of salt ions does not go beyond the first hydration layer; hence, the ionic influence is localized. Moreover, for the description of the complex *equilibrium* that takes place between the different solvation shells, "dynamic" effects should be taken into account: far from being static, the hydration layer changes in time, due to rotations and exchanges of water molecules. As the water molecule rotates, a tentative breaking or weakening of ion−water HB occurs. As the water molecules exchange layer, a reorganization of the hydrogen-bonding network also occurs. To this extent, structure sensitive computational and experimental methods can be very useful in unraveling the structure and dynamics of ionic hydration.

Among computational techniques, molecular dynamics (MD) simulations are very useful in revealing instantaneous molecular structures and dynamics in solution phases, as they allow for observation times spanning a noticeably extended range, from hundredths of picoseconds up to several nanoseconds. Within this range, both molecular (vibrational, rotational, etc.) and collective (shell residence times, solvent librations, HB network formation, etc.) dynamic properties can be computed and observed. Indeed, the reliability of the scenario described by MD techniques strongly depends upon the model adopted to mimic the molecular structure and interactions, which is in turn enclosed in the adopted force-field (FF). In the simulation of solvated ions, a key feature is

Received: November 13, 2014
Revised: November 19, 2014
Published: November 19, 2014

dx.doi.org/10.1021/jp511391b | J. Phys. Chem. B 2014, 118, 14899−14912

certainly a correct description of the electrostatic interaction between the ion and the surrounding water molecules. For this reason, to grant the required accuracy, the point charges should be accurately determined, possibly for the specific investigated species. Moreover, for a reliable comparison with the experimental vibrational spectra, the adopted FF should also allow for a sound description of the ion flexibility.

As far as experimental methods are concerned, infrared (IR) spectroscopy plays a very important role in understanding the structure and dynamics of the solvated ions, since it exploits the high sensitivity of a vibrating permanent dipole to the electric field of the IR radiation. As a consequence, both transition frequency and intensity of a given molecular vibrational mode are very sensitive to the electrostatic embedding of the atoms involved in the vibration. Moreover, as nearby water molecules move, the chemical environment of the monitored species may change, and this also reflects on its vibrational response. This makes IR spectroscopy a structure and dynamics sensitive method. Indeed, information about water structure and dynamics can be either directly evinced from the frequency change in water molecule vibrations, or indirectly obtained from the variation in vibrational frequencies (and intensities) of the hydrated ion. Recent ultrafast nonlinear IR methods, in particular two-dimensional infrared (2D IR) spectroscopy, have been extensively used to examine both the behavior of salt ions and the surrounding water molecules.[11−18] Additionally, the time scale of the nonlinear IR methods matches perfectly with the short time region of the aforementioned MD simulation range.

Cyanide ions are very popular models for studying ion solvation dynamics.[19−22] IR methods have been used to study the structure and dynamics of species containing a single cyanide[19,23] as well as multiple cyanides.[18,24−26] In particular, ferrocyanide ($[Fe(CN)_6]^{4-}$) and ferricyanide ($[Fe(CN)_6]^{3-}$) ions both have the same highly symmetric structure (O_h) but different charge distributions. These differences provide an interesting case to examine the structure and dynamics of anions in aqueous phase. Further, the cyanide stretch is located in an IR frequency window that does not overlap with that of water. The multiple probes present in cyano-ferrates are very sensitive to the solute−solvent interactions, from which the anion−water interaction can be studied. Similar case studies have been reported recently for tricyanomethanide[27] and guanidinium.[28] The vibrational energy levels and frequency shifts as well as vibrational relaxation pathways of the cyano-ferrates have been studied previously.[29,30] In a very recent work,[18] we have investigated the hydration structures and dynamics of cyano-ferrate anions in light and heavy water by using the 2D IR method.[18] The experimental results were interpreted in the light of different HB strengths between the ferro- and ferricyanide with the solvent, caused by the different charge distributions within the two ions. In particular, the experimental results were interpreted hypothesizing that water molecules in the hydration shell of the ferro species are more tightly bound to the cyano groups with respect to the ferri species. An important consequence of this hypothesis would be that, within the hydration shell, the $[Fe(CN)_6]^{4-}$ has a higher tendency to break water structure than ferricyanide.

In this work, we present a combined experimental/computational approach that integrates 2D IR spectroscopic measures with quantum mechanical (QM) and MD calculations, aimed to further understand the detailed hydration structures and dynamics of cyano-ferrate anions and to confirm some of the conclusions given in ref 18. Furthermore, exploiting the long time scale explored by MD, a rationalization of some open questions that arose in the above-referenced work will be given. For instance, previous results did not completely clarify whether the observed anisotropy decay is more likely to be associated with the physical rotation of the whole hydrated complexes, or rather with pseudorotations induced by the solvent through the so-called "dipolar reorientation", i.e., relaxation mechanisms between vibrational degenerate modes.[26,31] With these goals, 2D IR experimental spectra will be analyzed and interpreted in the light of MD simulations. These will be performed with accurate FFs, specifically suited for the two ions through the following procedure: (i) the FF point charges were refined specifically for each ion using QM calculations, purposely performed on the investigated systems; (ii) the intramolecular part of the FF was also specifically parametrized over QM computed data, exploiting the JOYCE protocol.[32,33] This should allow us to achieve the required accuracy in the description of electrostatic interactions and to reliably account for ion flexibility. Indeed, although never applied on ions, the JOYCE procedure has proven capable[32−40] of an accurate description of the vibrational features of several molecules in different complex environments.

The paper is organized as follows. First, computational and experimental methods are briefly described. Next, after a short discussion regarding the validity of the specifically parametrized FF, the computational results will be discussed in terms of structure and dynamic properties of the two ions. This virtual scenario will be employed to rationalize the experimental IR measurements presented here and recent literature results. Eventually, 1D and 2D IR spectra, computed from MD trajectories, will be compared with their measured counterparts, for a final validation of the present integrated computational−experimental study.

METHODS

QM and MD Calculations. All QM calculations were performed with the Gaussian09[41] software, using the B3LYP density functional coupled with 6-31+G* basis set. The lanl2dz pseudopotential was used for the Fe atom. The equilibrium geometry and the Hessian matrix were computed for both $[Fe(CN)_6]^{3-}$ and $[Fe(CN)_6]^{4-}$ ions after energy optimizations and inspection of the vibrational frequencies. MD simulations of systems consisting of one $[Fe(CN)_6]^{4-}$ (or $[Fe(CN)_6]^{3-}$) ion, four (or three) K^+ counterions, and 1297 water (or heavy water) molecules were performed for more than 10 ns with the Gromacs4.5[42] engine in the NPT ensemble, at 298 K and 1 atm. Further details on QM and MD calculations are given in the Supporting Information.

Force Fields. A specific parametrization was adopted for each cyanide ion. The parameters for the bonded coordinates were separately obtained for each anion, specifically tailoring the intramolecular description, through the JOYCE[32,33] procedure. Hence, a completely harmonic diagonal FF was parametrized from the QM computed data (optimized geometry and Hessian matrix) and employed for describing intramolecular flexibility, according to

$$E_{\text{intra}} = \frac{1}{2}\sum_{i=1}^{Ns} K_i^{s}(r_i - r_i^{0})^2 + \frac{1}{2}\sum_{i=1}^{N_b} K_i^{b}(\vartheta_i - \vartheta_i^{0})^2 + \frac{1}{2}\sum_{i=1}^{N_d} K_i^{d}(\varphi_i - \varphi_i^{0})^2 \quad (1)$$

The three sums are referred to stretching, bending, and torsional internal coordinates. As far as the nonbonded parameters are concerned, the interaction of each atom of the two anions with both the solvating water atoms and with the K^+ counterions is mimicked through a sum of 12-6 Lennard-Jones (LJ) and a standard Coulomb potential. LJ parameters were transferred for Fe from ref 43, whereas for C and N atoms they were taken from ref 44. On the contrary, an ad hoc parametrization was adopted for point charges, which were computed through the CHelpG fitting procedure for each ion in its QM optimized geometry.

For the description of the surrounding environment, the intermolecular FF parameters of K^+ counterions were taken from ref 45, while for H_2O the SPC/Fw[46] parameters were adopted. This latter choice was essentially due to the capability of the SPC/Fw model to account for water flexibility, which may be important for an accurate description of the anion vibrational features. Finally, as far as the D_2O solvent is concerned, two different sets of intermolecular parameters were tested. The first set is still SPC/Fw (with the deuterium mass doubled with respect to the hydrogen), whereas the other one is the SPC/HW model, developed by Grigera,[47] and recently validated in ref 48 for several D_2O bulk properties, over an extended range of temperatures. This latter model differs from the original SPC parametrization in the point charges, that are set to −0.87 and 0.435 (instead of −0.82 and 0.41) for oxygen and deuterium atoms, respectively. The intermolecular parameters of all water and heavy water models employed are reported in detail in Table T1 in the Supporting Information. Finally, it may be worth noticing that, for a more reliable comparison between H_2O and D_2O solvents, the same intramolecular parameters[46] were employed for all water models, even though the original SPC/HW parametrization does not account for molecular flexibility.

Trajectory Analysis. The water structure embedding the anion was investigated for each system by computing both standard center of mass-center of mass [$g(r)$; between ion and water] and atom−atom [$g_{kl}(r)$; between atom k of the ion and atom l of the solvent] pair correlation functions. Further information on the structural modifications induced by different environments on each anion was obtained by monitoring the distribution of selected internal coordinates. As far as the ion dynamics is concerned, 5 ns NVE trajectories were employed in the analysis of both translational and rotational diffusion, investigated by computing diffusion coefficients (D^{transl} and D^{rot}, see Supporting Information for details). Moreover, to gain a deeper insight into the reorientational behavior of the solvated ions, the relaxation of each molecular axis $\hat{u}_k$ ($k = a, b, c$; see Figure 1) was monitored through the following autocorrelation function (acf):

$$C_k^2(t) = \langle P_2[\hat{u}_k(t_0)\cdot\hat{u}_k(t + t_0)]\rangle \quad (2)$$

Here P_2 is the second Legendre polynomial. The resulting acf was thereafter fitted in a 5−25 ps window by a single exponential

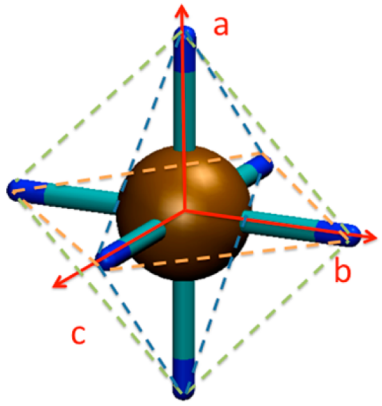

Figure 1. Equilibrium geometry computed for the $[Fe(CN)_6]^{3-}$ anion. The dashed lines show the three planes formed in the symmetric octahedral arrangement. The principal axes a, b, and c (solid red arrows) correspond to the three degenerate eigenvalues of the inertia tensor. A similar geometry (see text) was found for the $[Fe(CN)_6]^{4-}$ anion.

$$C_k^2(t) \approx e^{-\left(\frac{t}{\tau_k^R}\right)} \qquad k = a, b, c \quad (3)$$

Since both ions are expected to behave as spherical tops, the rotational relaxation time τ^R, connected to the overall molecular rotation, was eventually obtained by averaging the values obtained for each inertia axis k.

Finally, the vibrational behavior of the solvated ions was preliminarily investigated by computing the power spectrum $P(\omega)$ of the velocity acf of a single atom. Since the specific IR marker of the cyanide ions is the CN stretching mode, N atoms were chosen, as they are the most involved atoms in this specific motion. Therefore, for each of the four investigated systems, the Fourier transform of N velocity acf was performed over the NVE stored trajectories. It may be worth pointing out, as detailed in the Supporting Information (Figures S10 and S11), that identical CN frequencies are obtained when considering the power spectra obtained from the velocity acf's of other N or C atoms or any linear combination of them.

2D IR Computed Spectra. To account for anharmonicity effects, the CN stretching energy profile was determined with QM calculations, performed at the same level of theory adopted in FF parametrization, by optimizing all internal coordinates but the investigated CN bond length, which was increased stepwise in the 1.0−1.4 Å range. The resulting stretching profile was fitted with a Morse potential function. Exploiting the analytic solutions of the Schrödinger equation for a Morse oscillator, the frequency−frequency correlation function (FFCF) was computed from NVE MD trajectories. Finally, 2D IR spectra were calculated from FFCF following a slightly modified version of the protocol proposed by Hamm and coworkers.[19,49] Further details are given in the Supporting Information.

2D IR Experimental Spectra Processing. The femtosecond 2D IR spectra were collected as described previously.[18,50] Briefly, four mid-IR pulses were used to acquire the stimulated three-pulse vibrational photon echo. The delay time between the first and second pulses (k_1 and k_2) is the coherence time (τ) and that between the second and third pulses (k_2 and k_3) is the waiting time (T). The echo signal was detected in the $-k_1 + k_2 + k_3$ phase-matching direction. The four laser pulses were set to vertical polarization for parallel 2D IR measure-

dx.doi.org/10.1021/jp511391b | J. Phys. Chem. B 2014, 118, 14899−14912

ment. The collected signal is in the form $S_{re}(\tau, T, \omega_t)$ with $\tau > 0$ for rephasing and $S_{nr}(\tau, T, \omega_t)$ with $\tau \leq 0$ for nonrephasing. In a typical 2D IR experiment, for a given T time, τ was scanned for 2 ps with 5 fs step.

Two ways are used to process the collected 2D IR data in the present work. In the first case, numerical Fourier transform (FT) along the τ-axis yielded the frequency domain rephasing and nonrephasing 2D IR spectra, i.e., $S_{re}(-\omega_\tau, T, \omega_t)$ and $S_{nr}(\omega_\tau, T, \omega_t)$. Equally weighted rephasing and nonrephasing spectra yield a purely absorptive spectrum in the frequency domain. A series of T-dependent 2D IR spectra were obtained. In the second case, for a given T time, the rephasing and nonrephasing signals are merged along the τ-axis, and then the signals are summed along the ω_t-frequency axis:

$$S(\tau, T, \omega_t) = \sum_{\omega_t} [S_{re}(\tau, T, \omega_t) + S_{nr}(\tau, T, \omega_t)] \quad (5)$$

The resulting signal is equivalent to the three-pulse integrated photon echo reported previously.[51−53] The integration ranges of the ω_t-frequency for the ferro and ferri species are [2000−2070 cm^{-1}] and [2090−2120 cm^{-1}], respectively.

RESULTS

FF Parametrization. JOYCE[32,33] parametrization procedure was performed on both ions on the basis of QM optimized geometries and Hessian matrices. Both ions resulted in a symmetric octahedral arrangement, showing only small deviations in the bond lengths (less than 0.05 Å) and bond angles (less than 1°). The optimized $[Fe(CN)_6]^{3-}$ geometry is displayed in Figure 1.

In the FF parametrization, 0.017 $Å^4$ amu^2 and 0.008 $Å^4$ amu^2 standard[33−35,39,40] weights were employed for diagonal and off-diagonal Hessian elements, respectively.

The resulting standard deviations with respect to the QM data were comparable, being 3.2×10^{-3} kJ/mol and 3.1×10^{-3} kJ/mol for $[Fe(CN)_6]^{3-}$ and $[Fe(CN)_6]^{4-}$ ions, respectively. The final FF bonded parameters are reported in Table 1.

Table 1. Bonded FF Parameters Obtained with JOYCE[32,33] Parameterization for the Two Ions

	$[Fe(CN)_6]^{3-}$		$[Fe(CN)_6]^{4-}$	
bond	K^s (kJ/mol Å^{-2})	r_0 (Å)	K^s (kJ/mol Å^{-2})	r_0 (Å)
Fe−C	649.5	1.997	345.7	2.035
C−N	10 764.0	1.176	9954.6	1.186
angle	K^b (kJ/mol rad^{-2})	θ_0 (deg)	K^b (kJ/mol rad^{-2})	θ_0 (deg)
Fe−C−N	172.9	180.0	196.6	180.0
C−Fe−C	818.9	90.0/180.0	970.5	90.0/180.0
coplanar dihedral	K^d (kJ/mol rad^{-2})	φ_0 (deg)	K^d (kJ/mol rad^{-2})	φ_0 (deg)
C−C−C−C	354.4	0.0	454.8	0.0
N−N−N−N	354.4	0.0	454.8	0.0

As could be expected from the very similar QM optimized geometries, all equilibrium values of the internal coordinates show very small differences between the two anions. More precisely, the CN groups of the $[Fe(CN)_6]^{4-}$ complex show slightly larger equilibrium distances and are bound more loosely (i.e., smaller force constants) to the metal atom with respect to $[Fe(CN)_6]^{3-}$ complex. On the contrary, the bending and torsional constants in the ferrocyanide ion are somewhat larger. As a result, the "overall stiffness" of the molecular O_h structure is similar for the two cyanides. Conversely, as it appears from Table 2, the point charge distribution obtained from the

Table 2. CHelpG Charges Obtained at B3LYP/6-31+G* Level

atom	$[Fe(CN)_6]^{3-}$	$[Fe(CN)_6]^{4-}$
Fe	−0.834	−1.150
C	+0.403	+0.431
N	−0.763	−0.906

CHelpG procedure clearly distinguishes the two compounds. Therefore, it can be speculated that the major differences between the two ions can be ascribed to the electrostatic interaction with the environment rather than to geometrical or steric issues.

A first validation of the FF quality can be achieved by comparing the QM vibrational frequencies with those arising from the parametrized FF. As it appears from Figure 2, where

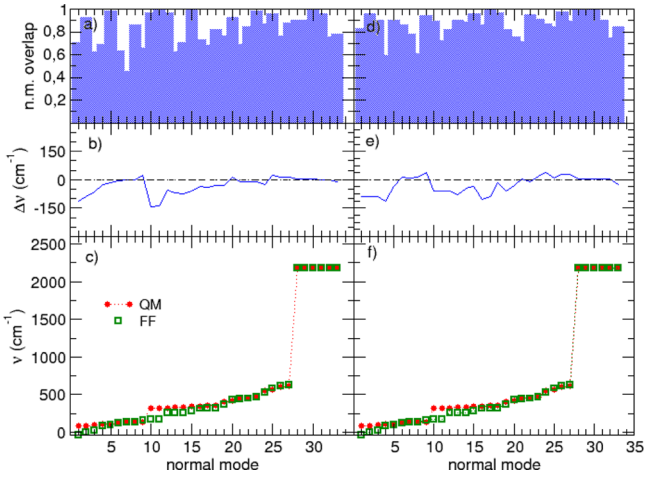

Figure 2. Frequency related results obtained with the JOYCE procedure for $[Fe(CN)_6]^{3-}$ (left) and $[Fe(CN)_6]^{4-}$ (right). From bottom to top: QM and FF vibrational frequencies (ν) for each normal mode; their difference $\Delta\nu$; overlap between QM and FF normal modes.

all QM and FF vibrational frequencies are reported together with their differences (middle panels) and the overlap of their normal modes (top panel), the agreement between QM values and FF ones is remarkable. As the CN stretchings will be the vibrations of reference for the present study, the agreement between the normal modes that they originate and those resulting from QM calculations is of particular interest. The modes involving the six equivalent local CN stretchings are found, for both ferro and ferri compounds, in the 2100−2200 cm^{-1} range and give rise to three distinct normal modes of A_{1g}, E_g, and T_{1u} symmetries. The latter is the only IR active mode, and it is clearly visible in the IR spectrum. An important feature of these six modes, which will be exploited in this paper, is that their frequencies are found in the 2087−2100 cm^{-1} and 2181−2194 cm^{-1} (for ferro- and ferri- ions, respectively) ranges; i.e., they are practically degenerate. This is a clear indication that the coupling between the local CN stretching modes is very low, being the normal modes essentially dictated by the O_h symmetry. The main consequence is that such vibrations can be treated using the normal modes or, equivalently, the local

dx.doi.org/10.1021/jp511391b | J. Phys. Chem. B 2014, 118, 14899−14912

modes, as they vibrate practically at the same frequency. The latter choice is much more convenient when the study is done using trajectories by MD and will be pursued in this paper, as detailed in the following. Such a feature is still conserved in case anharmonic terms are added to the vibrational Hamiltonian, as the frequency shift and the change in vibrational modes are not expected to alter the very weak coupling between the local modes. It is rather obvious that such an analysis is strictly referred to the frequencies of the power spectrum, with no reference to the intensity of vibrational transitions, which must be always treated in the context of normal modes, in order to get reliable results.

Structure. The two ion FFs, specifically parametrized for $[Fe(CN)_6]^{3-}$ and $[Fe(CN)_6]^{4-}$, were completed with the parameters chosen to mimic K^+ counterions and H_2O (or D_2O) solvent. It should be here mentioned that, as far as the different models tested for D_2O are concerned, the more reliable results (vide infra) were obtained when the SPC/Fw parameters were not varied. For this reason, all the following discussion on solvent effects regards the first heavy water model, whereas, for the sake of clarity, the results obtained with the SPC/Hw model are briefly discussed in the Supporting Information. NPT simulations were performed for each system, and the mass density was monitored over time until an equilibrium value was reached. Thereafter, 10 ns production runs were produced for each of the four systems. For comparison purposes, 10 ns NPT simulations were performed also on the pure H_2O and D_2O solvents.

The averaged densities are reported in Table 3 with their standard deviations. Regarding the pure solvents, the water density is in excellent agreement with the value reported in the SPC/Fw original paper[46] (1012 kg/m^3), slightly overestimating (1%) the experimental value (997 kg/m^3). Similarly, the D_2O water solvent shows an average density of 1121 kg/m^3, which also compares well with its experimental counterpart (1104 kg/m^3). Turning to the solvated ions, the presence of the cyanide species causes a ∼1.2% increase of the bulk density of both ferri and ferro systems. This value is in good agreement with the density increase measured experimentally for a $K_4[Fe(CN)_6]$ water solution of similar concentration.[54] The final equilibrated conformations of the four cyanide systems were used as starting points for production runs, in NPT and NVE ensembles. As detailed in the Supporting Information, NPT stored trajectories were employed to investigate structure properties, whereas conformations extracted from the NVE run were exploited in the calculation of ion translational, rotational, and vibrational dynamic behavior.

Solvation shells have been investigated through the calculation of the pair correlation function $g(r)$ between ion and water centers of mass, which is displayed in Figure 3.

Table 3. Average Mass Densities (ρ) Achieved in the NPT-MD Runs Performed on the Investigated Systems

system	ρ (kg/m^3)
H_2O	1008 ± 5
D_2O	1121 ± 6
$K_3[Fe(CN)_6]$@H_2O	1019 ± 5
$K_3[Fe(CN)_6]$@D_2O	1134 ± 5
$K_4[Fe(CN)_6]$@H_2O	1022 ± 5
$K_4[Fe(CN)_6]$@D_2O	1137 ± 5

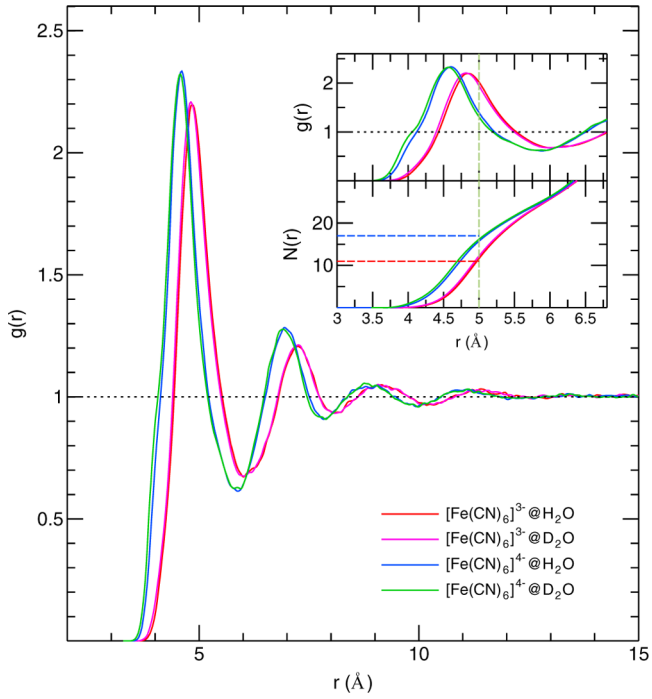

Figure 3. Pair correlation function $g(r)$ computed at 298 K and 1 atm for the four systems: $[Fe(CN)_6]^{3-}$ in water (red lines); $[Fe(CN)_6]^{3-}$ in heavy water (magenta); $[Fe(CN)_6]^{4-}$ in water (blue); $[Fe(CN)_6]^{4-}$ in heavy water (green). Inset: $g(r)$ and number of waters (N) at short distances. Horizontal dashed lines mark the number of solvent molecules within 5 Å.

In the inset, the number N of water molecules within the first shell is estimated from the integral of the first peak. It appears that, thanks to the higher charge, water molecules get closer to the $[Fe(CN)_6]^{4-}$ complex, with the peak position at around 4.6 Å, while the ferricyanide peak is found at ∼4.8 Å. This causes the less charged anion to be solvated by a larger shell, which extends up to ∼6.1 Å, whereas the radius of the first neighbors' shell for the $[Fe(CN)_6]^{4-}$ ions is ∼5.8 Å. Furthermore, as evidenced in the inset of Figure 3, water molecules in the first solvation shell of $[Fe(CN)_6]^{4-}$ are more closely "packed" near the ion, since the number of molecules found within 5 Å is 17 for $[Fe(CN)_6]^{4-}$ and 11 for $[Fe(CN)_6]^{3-}$. This scenario well matches the one outlined in ref 18, where ultrafast spectroscopy results were rationalized by hypothesizing a different strength of the ion−water interactions for the two ions, with the water molecules more tightly bound to the cyano groups for the ferro species. Finally, also in agreement with the previous findings, negligible differences are observed in the ions' structural features when comparing H_2O and D_2O solvents. Therefore, unless otherwise stated, all the following comments refer to both H_2O and D_2O solvents.

A deeper insight into the structure of the solvating environment of the two ions can be obtained by looking at the pair correlation functions $g_{kl}(r)$, computed for the N···Hw, Fe···Hw, and Fe···Ow pairs, being Hw and Ow hydrogen and oxygen water atoms, respectively. The $g_{N\cdots Hw}(r)$ pair correlation function is reported for all investigated systems in Figure 4. Only minor differences appear between the two ions, and negligible ones are again found between H_2O and D_2O. However, from a closer look at short distances (reported in the inset), a difference of ∼0.1 Å clearly emerges between the peak maxima of the two anions. In agreement with the scenario

dx.doi.org/10.1021/jp511391b | J. Phys. Chem. B 2014, 118, 14899−14912

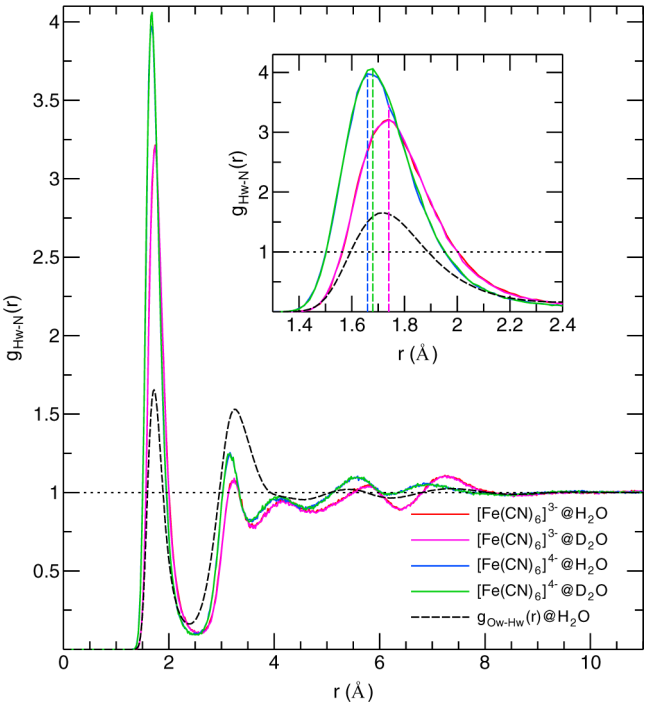

Figure 4. Atom−atom pair correlation function $g_{N\cdots Hw}(r)$ computed at 298 K and 1 atm for the four systems. Inset: $g_{N\cdots Hw}(r)$ at short distances. Dashed lines evidence the position of peak maxima for $[Fe(CN)_6]^{3-}$ (red) and $[Fe(CN)_6]^{3-}$ (blue). The $g_{Ow\cdots Hw}(r)$ pair correlation function, computed for pure H_2O, is displayed with dashed black lines.

described by the standard $g(r)$, water molecules are thus closer to the more charged ion, the most probable N···Hw distance being 1.68 Å for $[Fe(CN)_6]^{4-}$ and 1.74 Å for $[Fe(CN)_6]^{3-}$. Most important, both first neighbor peaks fall within the range expected for HB. To better compare the features of the HBs formed between the ions and the neighboring solvent molecules and those that take place in pure water, the $g_{Ow\cdots Hw}(r)$ pair correlation function between water hydrogen and oxygen atoms was computed over the pure H_2O trajectory and displayed in Figure 4. The resulting function is in good agreement with both literature and experimental data reported for H_2O (see ref 46 and references therein). Moreover, the comparison between $g_{Ow\cdots Hw}(r)$ and $g_{N\cdots Hw}(r)$ clearly shows that these functions have similar structure, with all peaks approximately centered at the same position. As evidenced in the inset, it is apparent that the HBs established by the ferri species lead to average N···Hw distances similar to those taking place between Ow···Hw pairs, whereas a smaller distance results for the ferro species. Further information on the local structure of the neighboring water molecules can be gained also by looking at the $g_{Fe\cdots Hw}(r)$ and $g_{Fe\cdots Ow}(r)$ atomic pair correlation functions, reported in the Supporting Information (Figure S1). Their inspection confirms that water molecules around the anion tend to orient their hydrogen atoms toward the cyanides, whereas oxygen ones are oriented toward the bulk. This mechanism is more efficient for the more charged ion, because the water molecules surrounding it are more closely packed. Hence, it can be inferred that within the first hydration shell ferro species breaks more water structure with respect to the ferri one.

The differences found in the pair correlation functions should reflect in a different HB network, established by the two species with the neighboring water molecules. By looking at Figure 5, where the number of HBs is computed as a function

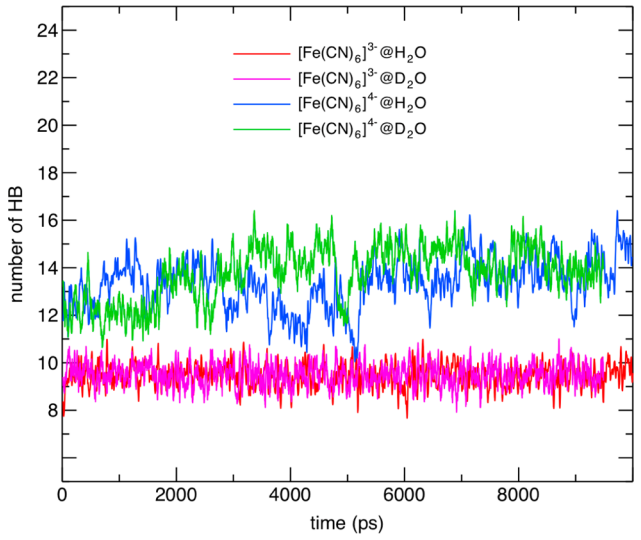

Figure 5. Number of HB for investigated species during the NPT simulation runs.

of simulation time for each ion in the two solvents, it appears that the scenario emerging from the $g(r)$'s analysis is fully confirmed. Indeed the number of HBs established by the more charged ion is always larger (∼13) than the one resulting for the ferri species (∼10).

While a more detailed analysis of the HB can be found in the Supporting Information (see Figures S2 and S3), here only the most important features will be commented on. First, as could be expected from the conclusions drawn so far, the residence times of D_2O (1.5 and 2.3 ps for $[Fe(CN)_6]^{3-}$ and $[Fe(CN)_6]^{4-}$, respectively) are similar to those found for H_2O (1.3 and 2.3 ps, respectively), whereas, within the same solvent, the surrounding water molecules spend more time on the ferro species with respect to the ferri ion. Furthermore, by looking at Figure S2 in Supporting Information, differences of about 0.1 Å are found in the donor (Ow)−acceptor (N) distances involving the two species, with shorter HBs found for the more charged ion.

The last investigated structural feature regards how the different solvation structures influence the geometry of the two complexes. This analysis concerns the population distributions of selected geometrical parameters, computed over the NPT trajectories. Among others, the Fe−C−N bending angle and the deviation χ from a perfect O_h structure are displayed in Figure 6. The latter parameter has been obtained by averaging over time the three dihedral angles formed by the quadruplets of C atoms coplanar in the equilibrium structure (see dashed lines in Figure 1), so that $\chi = 0$ indicates a perfectly symmetric O_h structure. It appears that the overall octahedral structure (i.e., the coplanarity of the three quadruplets) is well-maintained for both ions. Conversely, a different behavior of the two ions is found for the Fe−C−N bending angle. It should be pointed out that, thanks to the specificity of the employed parametrization procedure, the ferro and ferri FF have a different force constant connected with the Fe−C−N bending mode (see Table 1). As the Fe−C−N bending is characterized for both ions by a small force constant (less than 200 kJ/mol rad^{-2}), the population distribution of this internal coordinate is

dx.doi.org/10.1021/jp511391b | J. Phys. Chem. B 2014, 118, 14899−14912

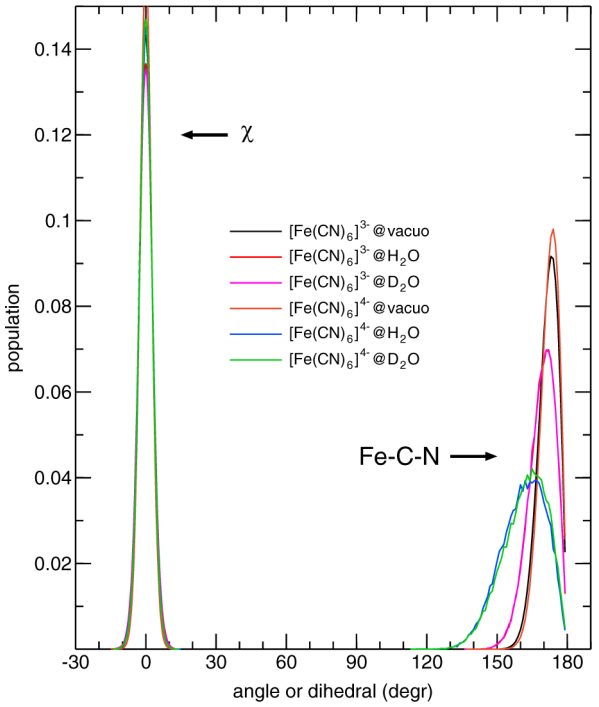

Figure 6. Population distributions at 298 K and 1 atm for selected geometrical parameters (left, deviation from planarity, χ; right, Fe−C−N bending angle distribution) of the two ions in H_2O/D_2O (red/magenta for $[Fe(CN)_6]^{3-}$ and blue/green for $[Fe(CN)_6]^{4-}$) and in vacuo (black and orange lines for $[Fe(CN)_6]^{3-}$ and $[Fe(CN)_6]^{3-}$, respectively).

expected to be rather sensitive to solvent perturbations. In fact, the distribution found for the more charged ion is broader and peaked around 160°, whereas the distribution found for $[Fe(CN)_6]^{3-}$ is narrower and centered around 170°. This difference cannot find an intramolecular rationale, as the smaller force constant of the ferri species (~170 vs ~200 kJ/mol rad^{-2} for the ferrocyanide) would suggest a slightly broader distribution for $[Fe(CN)_6]^{3-}$.

To verify this hypothesis, additional MD simulations were performed on the isolated ions (see Supporting Information for details), and the χ and Fe−C−N distributions were computed over a 10 ns trajectory at 298 K. By inspection of Figure 6, where the distributions in vacuo are also reported, it appears that both χ and Fe−C−N populations for the isolated ions do not present any remarkable difference between the two species. In particular the bending distributions are both peaked at ~180°, as could be expected from the harmonic potential driving the angle motions. Since the Fe−C−N distributions in solvent, in particular the one referring to $[Fe(CN)_6]^{4-}$, show a broader shape and are peaked to lower values, it can be inferred that the decisive effect on the computed distributions comes from the solvent; hence, it is of intermolecular nature. In fact, as indicated by the analysis of the pair correlation functions and of HBs, water molecules are at shorter distances from $[Fe(CN)_6]^{4-}$ than from the ferri ion, and a larger perturbation to the anion molecular shape is to be expected. This is also consistent with the higher interaction energies of the $[Fe(CN)_6]^{4-}/H_2O$ pair (~2000 kJ/mol vs ~1400 kJ/mol of the $[Fe(CN)_6]^{3-}/H_2O$ one).

Dynamics. As stated in the Methods section, the analysis of the ion's dynamics was performed on NVE trajectories. The translational dynamics of both ions was investigated in each solvent by monitoring the time dependence of the mean squared displacement (MSD) and the velocity acf. Both functions are displayed in Figure S4 of the Supporting Information. The D^{transl} coefficients were computed as half of the slope resulting from a linear fitting of the MSDs (in a 5−25 ps time window, where the ion has reached the diffusive regime), and their values are reported in Table 4.

Table 4. D^{transl} Coefficients Computed for the Ferri- and Ferrocyanide Ions in the Two Solvents[a]

	$[Fe(CN)_6]^{3-}$		$[Fe(CN)_6]^{4-}$	
D^{transl} (10^{-6} cm^2/s)	H_2O	D_2O	H_2O	D_2O
this work	4.3 ± 0.4	4.0 ± 0.3	3.6 ± 0.4	3.3 ± 0.3
expt[55,56]	[6.1−7.6]		[4.5−6.4]	

[a]Experimental ranges are also reported for comparison.

As could be expected from the previous discussion, in both solvents the more charged ion diffuses slightly more slowly, with 1.2 being the ratio between the two coefficients. Despite the few data available in the literature, the results in H_2O fairly agree with experimental findings[55,56] (see Table 4), with a slight underestimation. Most important, the ferri/ferro ratio is in quantitative agreement with the one evinced (1.2−1.3) from experimental data, confirming the faster dynamics for the ferri species.

The second observation that may be drawn is that the solvent plays a more relevant role in influencing the dynamic properties with respect to the structure ones. In fact, as far as translational diffusion is concerned, not negligible differences arise between H_2O and D_2O, with the dynamics of both ions in the latter solvent being slower than in the former one. The effect of deuteration can be ascribed in first approximation to several factors: the increased mass of the solvent molecules itself, the more efficient HB network, and/or the higher viscosity of D_2O.[47,48,57,58]

The rotational behavior of $[Fe(CN)_6]^{3-}$ and $[Fe(CN)_6]^{4-}$ was investigated by computing both diffusion coefficients, D^{rot}, and relaxation times, τ^R. In all cases, very similar values for the three considered axes (see Figure 1) were obtained for both D^{rot} and τ^R, confirming that both ions behave, as expected, as spherical tops. By looking at Table 5, where all the computed D^{rot} values (averaged over the three molecular axes) are reported, conclusions similar to translation can be drawn. Indeed, the quenching effect of heavy water is again evident: the HB formed by D_2O molecules with the N atom alters the inertia moment of the solvated complex, resulting in an overall decrease of the rotational diffusion coefficients. It may also be

Table 5. Rotational Diffusion Coefficients (10^9 s^{-1}) Computed for the Ferro- and Ferricyanide Ions in the Two Solvents[a]

system	solvent	$\langle D^{rot} \rangle$
$[Fe(CN)_6]^{3-}$	H_2O	4.5 ± 0.4
	D_2O	4.0 ± 0.5
$[Fe(CN)_6]^{4-}$	H_2O	3.8 ± 0.2
	D_2O	2.5 ± 0.6

[a]All values are averaged over the three molecular axes are indicated in Figure 1. The error was estimated from the sum of the squared deviations from the average of each value obtained for the considered molecular axes.

dx.doi.org/10.1021/jp511391b | J. Phys. Chem. B 2014, 118, 14899−14912

worth noticing that the effect of deuteration is more evident on the more charged ion, as previously found for translational dynamics.

Turning to rotational relaxation, both the effect of the heavy water and the quasi-isotropic rotation are confirmed by looking at the acf's of the molecular axes, reported in Figure 7. More

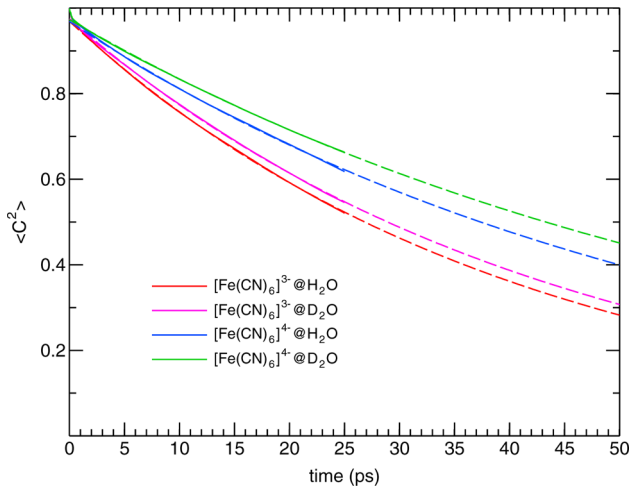

Figure 7. Rotational autocorrelation functions, computed according to eq 2 and averaged over the three molecular axes. The computed functions are shown with solid lines, whereas the single exponential fittings, see eq 3, are displayed with dashed lines.

specifically, in all systems the relaxation of every axis is rather slow, as the second Legendre polynomial does not vanish in the monitored time window. However, after 50 ps, the correlation is almost completely lost, as C^2 drops to 0.4 for the ferro species and below 0.3 for $[Fe(CN)_6]^{3-}$, confirming the faster rotational dynamics of the latter. It can be thus speculated that for both ions a complete randomization of the axis orientation, roughly corresponding to a complete molecular rotation, takes place on a few hundreds of picoseconds.

Rotational relaxation times, obtained from the single exponential fitting function and averaged over all three axes, are reported in Table 6. Similarly to translational and rotational

Table 6. Average Rotational Relaxation Times $\langle\tau^R\rangle$ (ps) Computed for All the Investigated Systems[a]

system	solvent	$\langle\tau^R\rangle$
$[Fe(CN)_6]^{3-}$	H_2O	41 ± 2
	D_2O	43 ± 2
$[Fe(CN)_6]^{4-}$	H_2O	57 ± 3
	D_2O	65 ± 4

[a]The error was estimated from the sum of the squared deviations from the average of each value obtained for the considered molecular axes.

diffusion coefficients, the rotational relaxation times also indicate that the rotational dynamics is slower in the D_2O solvent with respect to H_2O, with this effect being enhanced in the ferro case.

All τ^R values fall in between those computed for simple liquids (e.g., for liquid benzene[59] at 300 K: τ^R = 1.0−1.6 ps) and complex fluids (e.g., for a low molecular weight liquid crystal,[60,61] in its undercooled isotropic phase at 300 K, $\tau^R \approx$ 2000 ps). One possible interpretation is rooted in the HB formed between the ion and the neighboring (heavy) water molecules. Indeed, differently from a simple liquid, the water molecules that are H-bonded to anion's CN groups hamper its rotation. However, the water shells around the ion are less stable with respect to those formed in a partially ordered fluid (e.g., a liquid crystal), and the axis correlation disappears in shorter times. Comparing the rotational behavior of the ferro and ferri species, the different strength of the ion−water interactions can be again invoked to rationalize the present findings. Indeed, similarly to translational diffusion, as the water molecules are more closely bound to the $[Fe(CN)_6]^{4-}$ ion, the ferri species moves more freely, and the rotational relaxation process therefore is slightly faster. It is however important to note that both translational and rotational diffusion investigated phenomena span a rather extended time scale, and the hydrodynamic regime is probably reached only after several tens of picoseconds. This finding may contribute to the interpretation of the anisotropy decay measures, previously reported for ferro- and ferricyanide ions, which were found to be in the range of a few picoseconds.[18,24−26] It was hypothesized that the fast anisotropy decay could be due to rapid interchange between the degenerate vibrational modes, or alternatively to actual molecular rotation. Because the computations predict that actual molecular rotation occurs on a much longer time scale, the rapid decay observed experimentally could be assigned to the rapid relaxation between degenerate modes, as also proposed earlier.[26,31]

Frequency-Domain 2D IR Spectra. Two-dimensional IR spectroscopic measurements, previously[18] performed on water and heavy water solutions of both ions, are below discussed and interpreted on the basis of an integrated computational/experimental approach.

The 2D IR vibrational echo spectra in the C≡N stretching region for $[Fe(CN)_6]^{4-}$ and $[Fe(CN)_6]^{3-}$ in H_2O and D_2O, respectively, at two typical waiting times are shown in Figure 8 (top panel). The data of both ions in each solvent were collected simultaneously but plotted independently in Figure 8 in the desired spectral window. The $v = 0 \rightarrow v = 1$ (red) and $v = 1 \rightarrow v = 2$ (blue) transitions of the triply degenerate (T_{1u}) CN stretches clearly appear in the spectra. The ω_t-frequency separation between the red and blue signal in each case is assigned to the vibrational anharmonicity. The anharmonicity Δ is found to be 21.6 cm^{-1} for $[Fe(CN)_6]^{4-}$ and 18.6 cm^{-1} for $[Fe(CN)_6]^{3-}$ by fitting a slice of the 2D IR signal at 0.5 ps waiting time, along the ω_t axis with ω_τ set to 2D peak position. The evolution of the 2D IR peaks (shape and orientation) indicates the spectral diffusion process, which can be described by two-point frequency−frequency time-correlation function.[62]

Time-Domain 2D IR Data. From the line shape analysis, one can quantify the degree of elongation of the 2D IR signal and how the elongation evolves as a function of the waiting time T. Several approaches have been developed previously.[63−70] However, in this work a new approach is used to extract the frequency−frequency time-correlation function.

First, we re-treat the T-dependent 2D IR data by integrating the signal in selected frequency regions and plotting it as a function of τ. Both rephasing ($\tau > 0$) and nonrephasing ($\tau \leq 0$) signals are used. This yields the ω_t-integrated 2D IR signal. It is essentially identical to traditional three-pulse photon echo integrated over the t-time.[52,53] For a single IR chromophore, the integrating length can be the entire ω_t-axis. For a well-separated two-chromophore case, a limited range of frequency for each should be used. In this work, the ω_t-frequency for the ferro and ferri species are [2000−2070 cm^{-1}] and [2090−2120

dx.doi.org/10.1021/jp511391b | J. Phys. Chem. B 2014, 118, 14899−14912

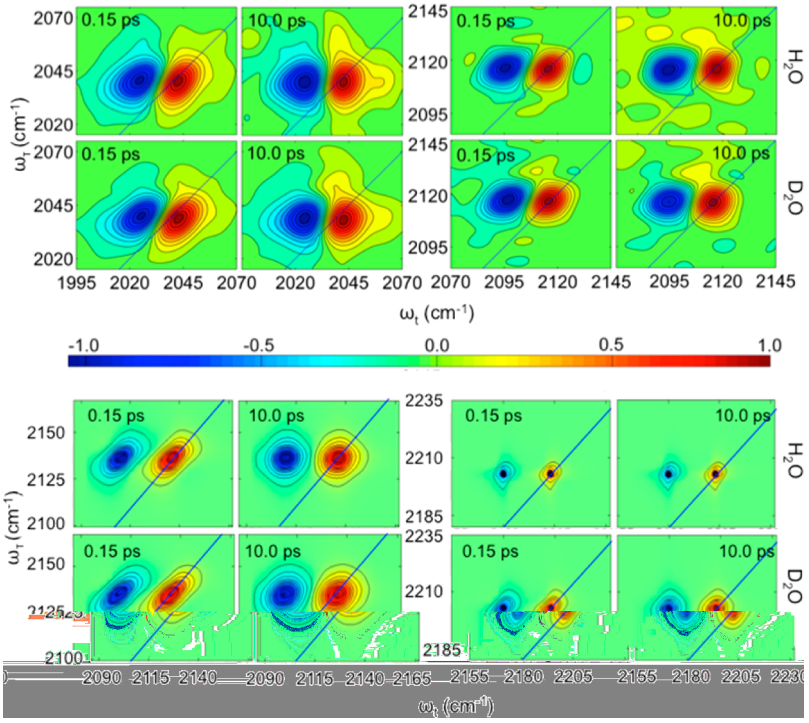

Figure 8. Top: Magnitude-normalized 2D IR vibrational echo spectra of the C≡N stretch of $[Fe(CN)_6]^{4-}$ (left) and $[Fe(CN)_6]^{3-}$ (right) in H_2O (upper) and in D_2O (lower) at selected waiting times T (0.15 and 10.0 ps). Adapted with permission from ref 18. Copyright 2014 American Chemical Society. Bottom: Magnitude-normalized 2D IR computed vibrational spectra of the C≡N stretch of $[Fe(CN)_6]^{4-}$ (left) and $[Fe(CN)_6]^{3-}$ (right) in H_2O (upper) and in D_2O (lower) at selected waiting times.

cm^{-1}], respectively. Figure 9 shows the reconstructed three-pulse photon echo signal of the cyano stretch for the $[Fe(CN)_6]^{4-}$ and $[Fe(CN)_6]^{3-}$ in H_2O and D_2O, respectively. Then the rephasing/nonrephasing ratio (RNR) is defined as

$$\mathrm{RNR}(T) = A_{re}(T)/A_{nr}(T) \quad (10)$$

where $A_{re}(T)$ and $A_{nr}(T)$ are integrated areas of the integrated three-pulse 2D IR signal with $\tau > 0$ for rephasing and $\tau \leq 0$ for nonrephasing. The obtained RNR as a function of T time is given in Figure 10.

The results are fitted using single-exponential function, and the fitted parameters are listed in Table 7.

The results show that the amplitude values are *ca.* 0.68−0.72 for the ferro species, and ca. 0.27−0.30 for the ferri species. Note that these amplitudes are relative and can be different from method to method. However, the amplitudes derived from the same method can be used to quantitatively describe the relative amount of the inhomogeneous broadening. The results shown in Table 7 suggest that the RNR method seems to be a more reasonable description of the relative inhomogeneous contribution for the two cases, because the values in H_2O and in D_2O are more consistent than previously estimated (also listed in Table 7).[18] Thus, it is concluded that the inhomogeneous content in the ferro species is roughly twice as much as in the ferri species. As for the FFCF dynamics, Table 7 indicates that even though there are some discrepancies between the values estimated in the present work and those from the slope method used in ref 18, the spectral diffusion occurs in 1−2 ps for the four systems, and the diffusion process is relatively slower in D_2O than in H_2O for each anion (1.7 ps in D_2O and 0.9 ps in H_2O for the ferri species, and 2.0 ps in D_2O and 1.4 ps in H_2O for the ferro species). In conclusion, we believe that $RNR(T)$ can be used as a more reliable measure of

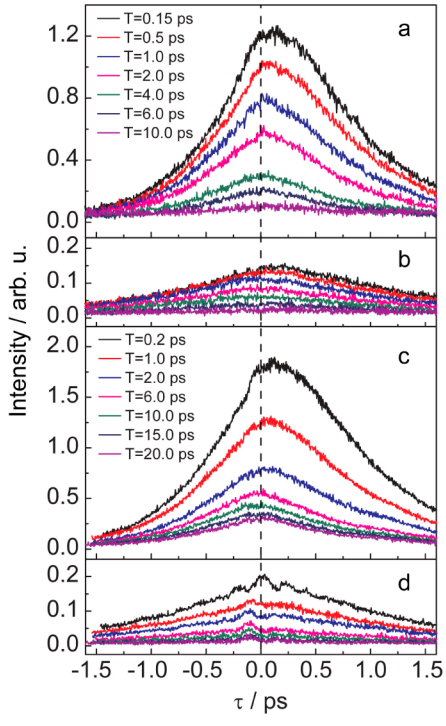

Figure 9. Reconstructed three-pulse photon echo signal of the cyano stretch at representative T times: (a) $[Fe(CN)_6]^{4-}$ in H_2O with T times given; (b) $[Fe(CN)_6]^{3-}$ in H_2O with the same T times as in part a; (c) $[Fe(CN)_6]^{4-}$ in D_2O with T times given; (d) $[Fe(CN)_6]^{3-}$ in D_2O with the same T times as in part c.

the spectral diffusion. On the contrary, the peak shift as a function of T-time, as previously used,[52] is actually not a very

dx.doi.org/10.1021/jp511391b | J. Phys. Chem. B 2014, 118, 14899−14912

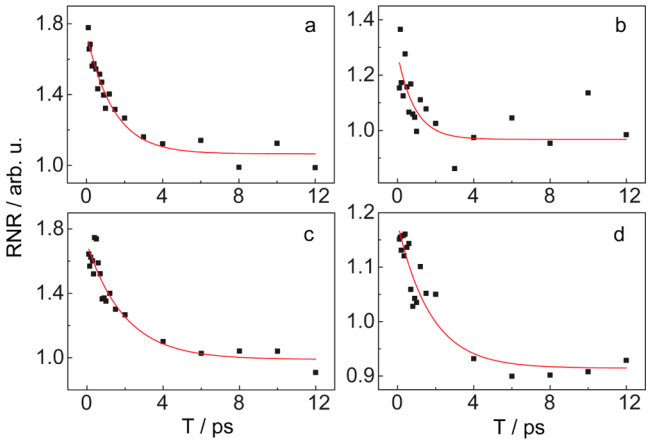

Figure 10. Rephasing/nonrephasing ratio from the ω_t-integrated 2D IR spectra as a function of T, and their single-exponential fits: (a) ferrocyanide in H_2O, (b) ferricyanide in H_2O, (c) ferrocyanide in D_2O, and (d) ferricyanide in D_2O.

Table 7. Fitting Parameters for the Rephasing/Nonrephasing Ratio as a Function of T-Time by Single Exponential Function for the C≡N Stretching of $[Fe(CN)_6]^{4-}$ and $[Fe(CN)_6]^{3-}$ Solvated in H_2O and in D_2O[a]

solute	solvent	A	$\tau_{SD}{}^1$/ps	$\tau_{SD}{}^2$/ps
$[Fe(CN)_6]^{3-}$	H_2O	0.30		0.9 ± 0.3
		0.15[d]		1.1 ± 0.4[b]
	D_2O	0.27		1.7 ± 0.4
		0.15[d]		1.5 ± 0.2[b]
$[Fe(CN)_6]^{4-}$	H_2O	0.68		1.4 ± 0.2
		0.24[d]		1.6 ± 0.2[b]
			0.08[c]	1.4[c]
	D_2O	0.72		2.0 ± 0.5
		0.30[d]		1.6 ± 0.2[b]
			0.08[c]	1.5[c]

[a]Values of FFCF dynamics from literatures are also listed for comparison. A is amplitude. [b]Results from ref 18 reported for comparison. [c]Results from ref 25. [d]Amplitude evaluated from ref 18 reported for comparison.

good measure of the spectral diffusion dynamics. A simple reason is that the information content from signal intensity is not fully utilized in the peak-shift method. Further, the $RNR(T)$ method is particularly useful when evaluating the spectral dynamics from weak 2D IR signal, such as the case of ferri species in this study.

One further important feature emerges from the analysis of these data. The observation that in both solvents the spectral diffusion of the less charged ferri species is faster than the one registered for the ferro homologue is in line with the faster dynamics observed in MD calculations, and supports the scenario where stronger interactions with the solvent tend to restrain the ion dynamics. In addition, it should be pointed out that the spectral diffusion dynamics given in Table 7 were evaluated by single exponentials. If a double exponential function were applied, a slow decay component (with time constant of tens of picoseconds in relatively larger uncertainty, and amplitude of roughly 10% of the total) could be obtained (data not shown). However, the time constants for the fast components remain quite similar to the results of the single exponential fitting. This implies the presence of a slow spectral diffusion process in all cases, which is in accordance with theoretical predictions (see below).

Computed 2D IR Spectra. A final validation of the conclusions drawn from the combined analysis presented so far can be achieved by a vis-à-vis comparison of the computed and measured 2D IR spectra.

Preliminary information on the vibrational behavior of the two ions can be gathered by looking at the power spectra $P(\omega)$ of the velocity acf computed for the N atom in the four systems. Furthermore, to better assess the role of the solvent, the trajectories in vacuo for both ions were also exploited to compute the power spectra for the isolated ions. All computed $P(\omega)$ values are displayed in Figure 11.

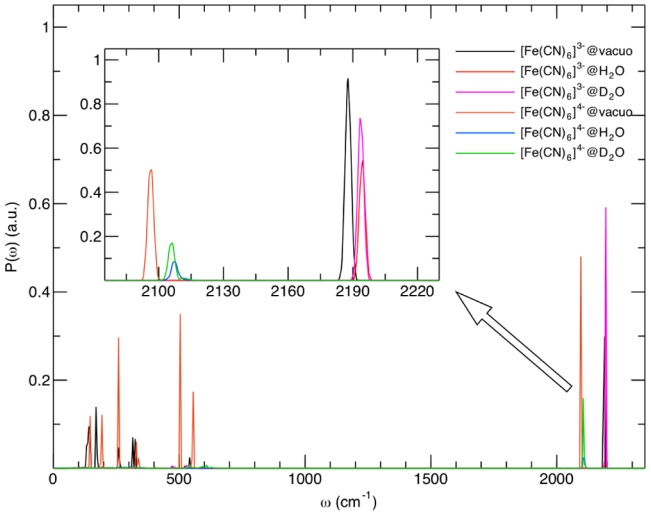

Figure 11. Power spectra of the N velocity acf, computed for the two ions in vacuo and in the different solvents. Inset: Blow up of the CN stretching region.

By looking at the power spectra computed in vacuo, it appears that the accuracy of the JOYCE FF parametrization is once again confirmed. Indeed, all computed $P(\omega)$ peaks coincide with the main IR frequencies, resulting from the reference QM calculation. Most important, as evidenced in the inset, the peaks connected to the CN stretching for the ferro and ferri species fall at 2093 and 2185 cm^{-1}, respectively, i.e., in excellent agreement with the QM computed IR frequencies (2087 and 2181 cm^{-1}) corresponding to the optically active T_{1u} symmetry modes. Turning to the power spectra computed for the solvated ions, they are found blue-shifted with respect to their in vacuo counterparts, and less intense, due to the smaller atom velocities, hampered by the solvent. It is important to notice that the shift due to the HB established with the neighboring solvent molecules (in the order of 10 cm^{-1}) is not larger than the coupling found between the ions' degenerate modes, hence the local mode picture also holds in the analysis of the vibrational behavior of the solvated ions.

From the comparison of the computed peaks in solvent, marked differences appear with respect to the scenario that emerged from the analysis of the translational and rotational dynamics, which take place on a slower time scale. Indeed, the fast motion of the vibrating ions results are more affected by the local patterns of the neighboring molecules (in turn determined by the different charge distributions) rather than by the characteristics of the embedding *media*: the peaks registered in H_2O and D_2O solvents for the same ion are very similar,

dx.doi.org/10.1021/jp511391b | J. Phys. Chem. B 2014, 118, 14899−14912

whereas the two ion peaks are very distinguishable. Some of the main features of the $P(\omega)$ computed in solvent are summarized in Table 8.

Table 8. Vibrational Peak Positions and Full Width at Half Maximum Computed and Measured[18] for the Two Ions in Different Solvents

method	anion	solvent	frequency (cm^{-1})	fwhm (cm^{-1})
expt, FTIR	$[Fe(CN)_6]^{4-}$	H_2O	2039.9	16.5
		D_2O	2038.9	16.5
	$[Fe(CN)_6]^{3-}$	H_2O	2115.6	7.8
		D_2O	2115.6	8.2
comp, MD	$[Fe(CN)_6]^{4-}$	H_2O	2107	6
		D_2O	2106	6
	$[Fe(CN)_6]^{3-}$	H_2O	2194	3
		D_2O	2193	3

A first indication of the validity of the vibrational description achieved by calculations may come from the comparison of the computed data with the experimental 1D-IR spectrum,[18] also reported in Table 8. However, it should be first pointed out that a quantitative agreement between the absolute positions and bandwidths of the $P(\omega)$ computed peaks and the IR experimental frequencies should not be expected, since important effects as anharmonicity were not included neither in the FF nor in the reference QM data employed in the JOYCE parametrization. This notwithstanding, the differences between the vibrational behavior of the ferro and ferri compounds, together with those arising between the two solvents, are well-reproduced. First, the relative behavior of the two ions in the same solvent is accounted for with significant accuracy. Indeed, the measured blue shift in peak maxima (from the $[Fe(CN)_6]^{4-}$ to the $[Fe(CN)_6]^{3-}$ ion) is around 76 cm^{-1} in H_2O and 77 in D_2O, in good agreement with the picture emerging from the MD calculations, where the two peaks are found in the correct order and separated by 87 cm^{-1} for both solvents. Moreover, the ratio between the fwhm of the ferro and ferri peaks is around 2, for both measured and computed values. Finally, as experimentally found, negligible differences are found between the two solvents for both investigated species.

For the calculation of the 2D IR spectra, following the suggestions of Hamm and co-workers,[19,49] the FFCF was computed over the NVE trajectories as detailed in the Supporting Information. The computed anharmonic shifts Δ^{Morse} for both ions (22.8 and 26.1 cm^{-1} $[Fe(CN)_6]^{3-}$ and $Fe(CN)_6]^{4-}$, respectively) are in good agreement in magnitude and relative order with those determined by 2D IR experiment (18.6 and 21.6 cm^{-1}). The computed results are also close to those previously determined for an isolated cyanide (CN^-) stretch in water, both experimentally[22] (21.4 cm^{-1}) and theoretically[19] (22 cm^{-1}).

The resulting FFCF was fitted with an analytical function, consisting of a sum of four exponentials, one of which is modulated with an oscillatory function (see eq S12 and Figure S13 in the Supporting Information). All the fitting parameters are reported in the Supporting Information (Table T4). It may be worth noticing that two of the four employed exponentials (in particular the one modulated by the oscillatory function) only contribute to fit the FFCF function at very short times, whereas the long time behavior is well-described by the two slower decaying exponentials. FFCF and the long time component ($Ce^{-t/\tau C} + De^{-t/\tau D}$) of the analytical function employed in the fitting are displayed in Figure 12 for all

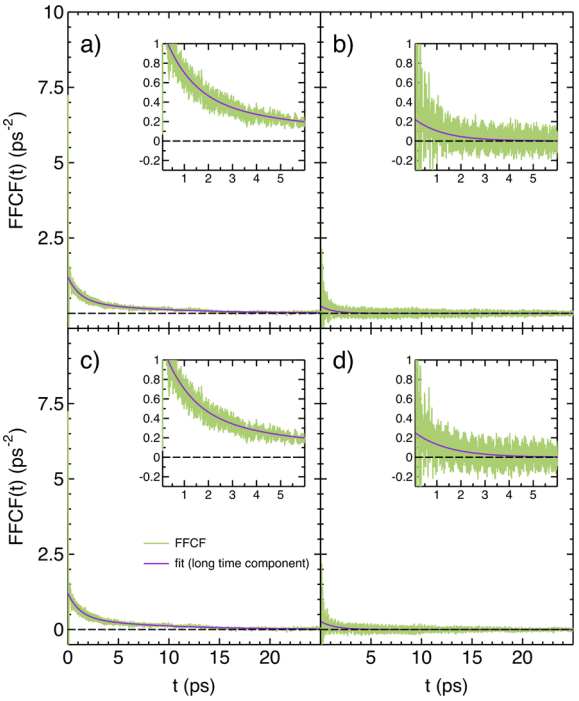

Figure 12. Computed FFCF functions (green) for the $[Fe(CN)_6]^{4-}$ (left) and $[Fe(CN)_6]^{3-}$ (right) ions in H_2O (top) and D_2O (bottom) solvents. The long time tails of the fitting functions reported in detail in eq S12 in Supporting Information are also displayed (violet lines). Insets: FFCF decay at short times.

systems, whereas behavior at very short times is displayed in Figure S13 in the Supporting Information. As a preliminary observation, most of the features of the experimental relaxation (see Figure 10) are well-reproduced. For instance, the computed FFCF confirms that the relaxation of $[Fe(CN)_6]^{3-}$ is the most rapid process and takes place within the first 3 ps, whereas the slowest decay is found for $[Fe(CN)_6]^{4-}$, that seems not completely ended after 10−15 ps. This is confirmed by the values obtained for the D coefficients (see Table T4 in the Supporting Information) for the two ions, since they are not negligible only for the ferro species, whereas they vanish when the faster ferri relaxation is considered. A possible rationale stands in the existence of a second slower relaxation process, that goes beyond the 1−5 ps scale vibrational relaxation and becomes more effective when stronger interactions with the solvent come into play.

By looking at the best-fit parameters and at the amplitudes connected to each exponential (reported in detail in the Supporting Information Table T4), it appears that the computed relaxation in the 1−5 ps region is essentially driven by the third, not oscillatory, exponential component ($Ce^{-t/\tau C}$) of the fitting function. Therefore, both amplitude C and relaxation time τ_C can be in first approximation compared to the parameters of the single exponential (A and τ_{SD}^2) employed to fit experimental data in Figure 10. By looking at Table 9, where the above-mentioned computed and experimental fit parameters are reported, the agreement between the experimental and computational description is rather good, confirming the reliability of the virtual scenario and the validity of the description evinced from the analysis of the experimental

dx.doi.org/10.1021/jp511391b | J. Phys. Chem. B 2014, 118, 14899−14912

Table 9. Best Fit Parameters for the Exponential Decay ($Ce^{-t/\tau C}$) of the FFCF in the 1−5 ps Region[a]

system	solvent	C (ps^{-2})	A (ps^{-2})	τ_C (ps)	τ_{SD}^2 (ps)
$[Fe(CN)_6]^{3-}$	H_2O	0.24 ± 0.02	0.30	1.2 ± 0.2	0.9 ± 0.3
	D_2O	0.27 ± 0.02	0.27	1.4 ± 0.3	1.7 ± 0.4
$[Fe(CN)_6]^{4-}$	H_2O	0.80 ± 0.08	0.68	1.2 ± 0.1	1.4 ± 0.2
	D_2O	0.85 ± 0.02	0.72	1.4 ± 0.3	2.0 ± 0.5

[a]More details of the employed fitting functions are reported in the Supporting Information. In the fourth and sixth columns the experimental amplitudes A and relaxation times τ_{SD}^2 measured in this work and already reported in Table 6 are also shown here for a more straightforward comparison.

spectra. As far as the solvent effect is concerned, the experimental increase of the relaxation times upon deuteration is also well-reproduced. A somewhat worse agreement to the experimental data is apparently found when the relative behavior of the two ions is considered, as the τ_C relaxation times for the ferro/ferri species are more similar to each other with respect to the experiment. However, inspection of Figure 12 clearly shows that the overall relaxation of the ferro compound is slower than the one found for the ferri homologue, since in the former case the contribution of the fourth exponential is not negligible. In addition, the amplitudes of the considered exponential decay agree well with the experimental ones, confirming the difference in inhomogeneous content experimentally found between the two species.

It may also be worth mentioning that the influence of the surrounding medium decays as the time scale spanned by the considered dynamic process increases. For instance, the vibrational faster processes (represented by $\tau_A-\tau_C$, see Table T4 in Supporting Information) show a much smaller dependence upon the solvent. This seems to confirm the conclusions drawn for translational and rotational motions, i.e., that the effect of deuteration becomes more evident as the dynamical process considered involves increasing time scales.

Finally, the 2D IR spectra were obtained from the computed FFCF, following the procedure reported in refs 19 and 49, as detailed in the Supporting Information and reported in the bottom panel of Figure 8. By comparing the experimental and computed 2D IR spectra shown in Figure 8, the good matching between the experimental and computational description clearly appears. Indeed, all the most important features observed in the experimental 2D IR spectra can also be found in the computed ones. (i) The spectral features registered for identical waiting times for the same ion in different solvents are very similar. This confirms that the role of the solvent is almost negligible in the picosecond time scale spanned by vibrational dynamics. (ii) All signals (except the one for ferricyanide ion in H_2O) are elongated along the diagonal at small waiting times, whereas a more symmetric shape is achieved in all cases at T = 10 ps.

CONCLUSIONS

In this work, information gathered from (2D) IR experimental measurements and the results achieved with MD simulations were integrated to achieve a deeper insight into the structure and dynamics of ferro- and ferricyanide ions in aqueous solution. First, accurate force-fields were specifically parametrized through the JOYCE procedure, to mimic the behavior of each species. Long lasting simulations for each ion in water and heavy water solvents were then performed to achieve a detailed description of the structural and dynamic patterns that characterized the two ions. The reliability of such description was evaluated through the successful comparison with the available experimental data, in particular the measured IR spectra. Computational results are found to reproduce well several key features the 2D IR spectra, including the overtone anharmonicities, spectral diffusion time, or FFCF dynamics and the contribution of inhomogeneous amplitudes. This agreement makes a joint analysis possible, as the IR spectral line shapes reflect the features that characterize solute−solvent interaction within the ion hydration shells.

As far as the subtle differences between the two ions are concerned, both computational and experimental results show that the frequency correlation function relaxes more slowly in the case of the ferrocyanide. A straightforward rationale stands in the fact that tighter hydrogen bonds are formed by the more charged ion, as confirmed by the analysis of computed pair correlation functions. The stronger interaction with the solvent is also suggested by the larger distortions from the octahedral symmetry found in ferrocyanide conformational distributions. Such a phenomenon is even more evident on slow dynamics, where the less interacting ferri species moves faster than ferro. As a matter of fact, both translational and rotational diffusion were found to be much more sensitive to solvent interactions than fast vibrational motion, with the dynamics in D_2O being slower that that computed in pure water. Furthermore, the computed relaxation times related to rotational dynamics indicate that the rotation of the overall molecule takes place on a 100 ps time scale. This observation helps in clarifying the analysis of the anisotropy decay, addressed in our previous work,[18] where it was hypothesized that this fast decay could be due to some interchange mechanism between degenerate modes, rather than to the rotation of the whole molecule. Considering the long rotational relaxation times indicated by the MD simulations, the above hypothesis can be confirmed, and measured reorientational short times are probably connected with a rapid interchange between the degenerate modes.

ASSOCIATED CONTENT

Supporting Information

Computation details and additional results. This material is available free of charge via the Internet at http://pubs.acs.org.

AUTHOR INFORMATION

Corresponding Author

*E-mail: giacomo.prampolini@pi.iccom.cnr.it.

Notes

The authors declare no competing financial interest.

ACKNOWLEDGMENTS

This work was supported by the Knowledge Innovation Program (KJCX2-EW-H01) and the Hundred Talent Fund of the Chinese Academy of Sciences (to J.W.), and also supported by the National Natural Science Foundation of China

(91121020, and 21103200). G.P. and S.P. are grateful to Dr. Fabrizio Santoro and Dr. Francisco J. Avila Ferrer for the many useful discussions and suggestions.

REFERENCES

(1) Ohtaki, H.; Radnai, T. Structure and Dynamics of Hydrated Ions. *Chem. Rev.* **1993**, *93*, 1157−1204.
(2) Marcus, Y. Effect of Ions on the Structure of Water: Structure Making and Breaking. *Chem. Rev.* **2009**, *109*, 1346−1370.
(3) Schwenk, C. F.; Hofer, T. S.; Rode, B. M. "Structure Breaking" Effect of Hydrated Cs^+. *J. Phys. Chem. A* **2004**, *108*, 1509−1514.
(4) Mancinelli, R.; Botti, A.; Bruni, F.; Ricci, M. A.; Soper, A. K. Perturbation of Water Structure Due to Monovalent Ions in Solution. *Phys. Chem. Chem. Phys.* **2007**, *9*, 2959−2967.
(5) Lyubartsev, A. P.; Laasonen, K.; Laaksonen, A. Hydration of Li^+ Ion. An Ab Initio Molecular Dynamics Simulation. *J. Chem. Phys.* **2001**, *114*, 3120−3126.
(6) Omta, A. W.; Kropman, M. F.; Woutersen, S.; Bakker, H. J. Negligible Effect of Ions on the Hydrogen-Bond Structure in Liquid Water. *Science* **2003**, *301*, 347−349.
(7) Omta, A. W.; Kropman, M. F.; Woutersen, S.; Bakker, H. J. Influence of Ions on the Hydrogen-Bond Structure in Liquid Water. *J. Chem. Phys.* **2003**, *119*, 12457−12461.
(8) Tielrooij, K. J.; Garcia-Araez, N.; Bonn, M.; Bakker, H. J. Cooperativity in Ion Hydration. *Science* **2010**, *328*, 1006−1009.
(9) Smith, J. D.; Saykally, R. J.; Geissler, P. L. The Effects of Dissolved Halide Anions on Hydrogen Bonding in Liquid Water. *J. Am. Chem. Soc.* **2007**, *129*, 13847−13856.
(10) Mancinelli, R.; Botti, A.; Bruni, F.; Ricci, M. A.; Soper, A. K. Hydration of Sodium, Potassium, and Chloride Ions in Solution and the Concept of Structure Maker/Breaker. *J. Phys. Chem. B* **2007**, *111*, 13570−13577.
(11) Moilanen, D. E.; Wong, D.; Rosenfeld, D. E.; Fenn, E. E.; Fayer, M. D. Ion−Water Hydrogen-Bond Switching Observed with 2D IR Vibrational Echo Chemical Exchange Spectroscopy. *Proc. Natl. Acad. Sci. U.S.A.* **2009**, *106*, 375−380.
(12) Son, H.; Jin, H.; Choi, S. R.; Jung, H. W.; Park, S. Infrared Probing of Equilibrium and Dynamics of Metal−Selenocyanate Ion Pairs in N,N-Dimethylformamide Solutions. *J. Phys. Chem. B* **2012**, *116*, 9152−9159.
(13) Fayer, M. D.; Moilanen, D. E.; Wong, D.; Rosenfeld, D. E.; Fenn, E. E.; Park, S. Water Dynamics in Salt Solutions Studied with Ultrafast Two-Dimensional Infrared (2D IR) Vibrational Echo Spectroscopy. *Acc. Chem. Res.* **2009**, *42*, 1210−1219.
(14) Bian, H.; Wen, X.; Li, J.; Chen, H.; Han, S.; Sun, X.; Song, J.; Zhuang, W.; Zheng, J. Ion Clustering in Aqueous Solutions Probed with Vibrational Energy Transfer. *Proc. Natl. Acad. Sci. U.S.A.* **2011**, *108* (12), 4737−4742.
(15) Tielrooij, K. J.; van der Post, S. T.; Hunger, J.; Bonn, M.; Bakker, H. J. Anisotropic Water Reorientation Around Ions. *J. Phys. Chem. B* **2011**, *115*, 12638−12647.
(16) Ji, M.; Odelius, M.; Gaffney, K. J. Large Angular Jump Mechanism Observed for Hydrogen Bond Exchange in Aqueous Perchlorate Solution. *Science* **2010**, *328*, 1003−1005.
(17) Singh, P. K.; Kuroda, D. G.; Hochstrasser, R. M. An Ion's Perspective on the Molecular Motions of Nanoconfined Water: A Two-Dimensional Infrared Spectroscopy Study. *J. Phys. Chem. B* **2013**, *117*, 9775−9784.
(18) Yu, P.; Yang, F.; Zhao, J.; Wang, J. Hydration Dynamics of Cyanoferrate Anions Examined by Ultrafast Infrared Spectroscopy. *J. Phys. Chem. B* **2014**, *118* (11), 3104−3114.
(19) Lee, M. W.; Carr, J. K.; Gollner, M.; Hamm, P.; Meuwly, M. 2D IR Spectra of Cyanide in Water Investigated by Molecular Dynamics Simulations. *J. Chem. Phys.* **2013**, *139*, 054506-1−054506-12.
(20) Lascombe, J.; Perrot, M. Structure and Motion in Water. Analysis of Vibrational and Rotational Dynamics of Cyanide Ion in Aqueous Solution from Infrared and Raman Bandshapes. *Faraday Discuss. Chem. Soc.* **1978**, *66*, 216−230.
(21) Hamm, P.; Lim, M.; Hochstrasser, R. M. Vibrational Energy Relaxation of the Cyanide Ion in Water. *J. Chem. Phys.* **1997**, *107*, 10523−10531.
(22) Koziński, M.; Garrett-Roe, S.; Hamm, P. Vibrational Spectral Diffusion of CN^- in Water. *Chem. Phys.* **2007**, *341*, 5−10.
(23) Rey, R.; Hynes, J. T. Vibrational Phase and Energy Relaxation of CN^- in Water. *J. Chem. Phys.* **1998**, *108*, 142−153.
(24) Ohta, K.; Maekawa, H.; Tominaga, K. Vibrational Population Relaxation and Dephasing Dynamics of $Fe(CN)_6^{4-}$ in D_2O with Third-Order Nonlinear Infrared Spectroscopy. *J. Phys. Chem. A* **2004**, *108*, 1333−1341.
(25) Ohta, K.; Maekawa, H.; Tominaga, K. Vibrational Population Relaxation and Dephasing Dynamics of $Fe(CN)_6^{4-}$ in Water: Deuterium Isotope Effect of Solvents. *Chem. Phys. Lett.* **2004**, *386*, 32−37.
(26) Sando, G. M.; Zhong, Q.; Owrutsky, J. C. Vibrational and Rotational Dynamics of Cyanoferrates in Solution. *J. Chem. Phys.* **2004**, *121*, 2158−2168.
(27) Kuroda, D. G.; Singh, P. K.; Hochstrasser, R. M. Differential Hydration of Tricyanomethanide Observed by Time Resolved Vibrational Spectroscopy. *J. Phys. Chem. B* **2013**, *117*, 4354−4364.
(28) Vorobyev, D. Y.; Kuo, C.-H.; Kuroda, D. G.; Scott, J. N.; Vanderkooi, J. M.; Hochstrasser, R. M. Water-Induced Relaxation of a Degenerate Vibration of Guanidinium Using 2D IR Echo Spectroscopy. *J. Phys. Chem. B* **2010**, *114*, 2944−2953.
(29) Kettle, S. F. A.; Aschero, G. L.; Diana, E.; Rossetti, R.; Stanghellini, P. L. The Vibrational Spectra of the Cyanide Ligand Revisited: Terminal Cyanides. *Inorg. Chem.* **2006**, *45*, 4928−4937.
(30) Watzky, M. A.; Endicott, J. F.; Song, X.; Lei, Y.; Macatangay, A. Red-Shifted Cyanide Stretching Frequencies in Cyanide-Bridged Transition Metal Donor−Acceptor Complexes. Support for Vibronic Coupling. *Inorg. Chem.* **1996**, *35*, 3463−3473.
(31) Tokmakoff, A.; Urdahl, R. S.; Zimdars, D.; Francis, R. S.; Kwok, A. S.; Fayer, M. D. Vibrational Spectral Diffusion and Population Dynamics in a Glass-Forming Liquid: Variable Bandwidth Picosecond Infrared Spectroscopy. *J. Chem. Phys.* **1995**, *102*, 3919−3931.
(32) Cacelli, I.; Prampolini, G. Parametrization and Validation of Intramolecular Force Fields Derived from DFT Calculations. *J. Chem. Theory Comput.* **2007**, *3*, 1803−1817.
(33) Barone, V.; Cacelli, I.; De Mitri, N.; Licari, D.; Monti, S.; Prampolini, G. Joyce and Ulysses: Integrated and User-Friendly Tools for the Parameterization of Intramolecular Force Fields from Quantum Mechanical Data. *Phys. Chem. Chem. Phys.* **2013**, *15*, 3736−3751.
(34) Cacelli, I.; Cimoli, A.; De Gaetani, L.; Prampolini, G.; Tani, A. Chemical Detail Force Fields for Mesogenic Molecules. *J. Chem. Theory Comput.* **2009**, *5*, 1865−1876.
(35) Cacelli, I.; Lami, C. F.; Prampolini, G. Force-Field Modeling through Quantum Mechanical Calculations: Molecular Dynamics Simulations of a Nematogenic Molecule in its Condensed Phases. *J. Comput. Chem.* **2009**, *30*, 366−378.
(36) Barone, V.; Bloino, J.; Monti, S.; Pedone, A.; Prampolini, G. Theoretical Multilevel Approach for Studying the Photophysical Properties of Organic Dyes in Solution. *Phys. Chem. Chem. Phys.* **2010**, *12*, 10550−10561.
(37) Barone, V.; Cacelli, I.; Ferretti, A.; Monti, S.; Prampolini, G. Parameterization and Validation of an Accurate Force-Field for the Simulation of Alkylamine Functionalized Silicon (111) Surfaces. *Phys. Chem. Chem. Phys.* **2010**, *12*, 4201−4209.
(38) Barone, V.; Bloino, J.; Monti, S.; Pedone, A.; Prampolini, G. Fluorescence Spectra of Organic Dyes in Solution: A Time Dependent Multilevel Approach. *Phys. Chem. Chem. Phys.* **2011**, *13*, 2160−2166.
(39) Cacelli, I.; Cimoli, A.; Livotto, P. R.; Prampolini, G. An Automated Approach for the Parameterization of Accurate Intermolecular Force-Fields: Pyridine as a Case Study. *J. Comput. Chem.* **2012**, *33*, 1055−1067.
(40) De Mitri, N.; Monti, S.; Prampolini, G.; Barone, V. Absorption and Emission Spectra of a Flexible Dye in Solution: A Computational Time-Dependent Approach. *J. Chem. Theory Comput.* **2013**, *9*, 4507−4516.

(41) Frisch, M. J.; Trucks, G. W.; Schlegel, H. B.; Scuseria, G. E.; Robb, M. A.; Cheeseman, J. R.; Scalmani, G.; Barone, V.; Mennucci, B.; Petersson, G. A.; et al. *Gaussian 09, Revision D.01*; Gaussian, Inc.: Wallingford, CT, 2009.
(42) van der Spoel, D.; Lindahl, E.; Hess, B.; van Buuren, A. R.; Apol, E.; Meulenhoff, P.; Tieleman, D.; Sijbers, A.; Feenstra, K.; van Drunen, R.; et al. *GROMACS4.5*; 2010.
(43) Aguilar, C. M.; De Almeida, W. B.; Rocha, W. R. The Electronic Spectrum of Fe2+ Ion in Aqueous Solution: A Sequential Monte Carlo/Quantum Mechanical Study. *Chem. Phys. Lett.* **2007**, *449*, 144−148.
(44) Price, M. L. P.; Ostrovsky, D.; Jorgensen, W. L. Gas-phase and Liquid-state Properties of Esters, Nitriles, and Nitro Compounds with the OPLS-AA Force Field. *J. Comput. Chem.* **2001**, *22*, 1340−1352.
(45) Aaqvist, J. Ion-Water Interaction Potentials Derived from Free Energy Perturbation Simulations. *J. Phys. Chem.* **1990**, *94*, 8021−8024.
(46) Wu, Y.; Tepper, H. L.; Voth, G. A. Flexible Simple Point-Charge Water Model with Improved Liquid-State Properties. *J. Chem. Phys.* **2006**, *124*, 024503−1−024503−12.
(47) Grigera, J. R. An Effective Pair Potential for Heavy Water. *J. Chem. Phys.* **2001**, *114*, 8064−8064.
(48) Bandyopadhyay, D.; Mohan, S.; Ghosh, S. K.; Choudhury, N. Properties of Heavy Water in the Temperature Range T = 223 to 373 K from Molecular Dynamics Simulation Using the Simple Point Charge/Heavy Water (SPC/HW) Model. *J. Chem. Eng. Data* **2012**, *57*, 1751−1758.
(49) Hamm, P.; Zanni, M. *Concepts and Methods of 2D Infrared Spectroscopy*; Cambridge University Press: New York, 2011.
(50) Li, D.; Yang, F.; Han, C.; Zhao, J.; Wang, J. Correlated High-Frequency Molecular Motions in Neat Liquid Probed with Ultrafast Overtone Two-Dimensional Infrared Spectroscopy. *J. Phys. Chem. Lett.* **2012**, *3*, 3665−3670.
(51) Hamm, P.; Lim, M.; Hochstrasser, R. M. Non-Markovian Dynamics of the Vibrations of Ions in Water from Femtosecond Infrared Three-Pulse Photon Echoes. *Phys. Rev. Lett.* **1998**, *81*, 5326−5329.
(52) Kim, Y. S.; Hochstrasser, R. M. Dynamics of Amide-I Modes of the Alanine Dipeptide in D_2O. *J. Phys. Chem. B* **2005**, *109*, 6884−6891.
(53) Park, J.; Hochstrasser, R. M. Multidimensional Infrared Spectroscopy of a Peptide Intramolecular Hydrogen Bond. *Chem. Phys.* **2006**, *323*, 78−86.
(54) Hood, G. R.; Williams, J. C. The Viscosity and Fludity of Aqueous Potassium Ferrocyanide Solutions. *Ohio J. Sci.* **1935**, *25*, 415−420.
(55) Konopka, S. J.; McDuffie, B. Diffusion Coefficients of Ferri- and Ferrocyanide Ions in Aqueous Media, Using Twin-Electrode Thin-Layer Electrochemistry. *Anal. Chem.* **1970**, *42*, 1741−1746.
(56) Gerhardt, G.; Adams, R. N. Determination of Diffusion Coefficients by Flow Injection Analysis. *Anal. Chem.* **1982**, *54*, 2618−2620.
(57) Okada, K.; Yao, M.; Hiejima, Y.; Kohno, H.; Kajihara, Y. Dielectric Relaxation of Water and Heavy Water in the Whole Fluid Phase. *J. Chem. Phys.* **1999**, *110*, 3026−3036.
(58) Sheu, S.-Y.; Schlag, E. W.; Selzle, H. L.; Yang, D.-Y. Molecular Dynamics of Hydrogen Bonds in Protein-D2O: the Solvent Isotope Effect. *J. Phys. Chem. A* **2008**, *112*, 797−802.
(59) Cacelli, I.; Cinacchi, G.; Prampolini, G.; Tani, A. Computer Simulation of Solid and Liquid Benzene with an Atomistic Interaction Potential Derived from Ab Initio Calculations. *J. Am. Chem. Soc.* **2004**, *126*, 14278−14286.
(60) De Gaetani, L.; Prampolini, G.; Tani, A. Anomalous Diffusion and Cage Effects in the Isotropic Phase of a Liquid Crystal. *J. Phys. Chem. B* **2007**, *111*, 7473−7477.
(61) De Gaetani, L.; Prampolini, G.; Tani, A. Modeling a Liquid Crystal Dynamics by Atomistic Simulation with an Ab Initio Derived Force Field. *J. Phys. Chem. B* **2006**, *110*, 2847−2854.
(62) Piryatinski, A.; Skinner, J. L. Determining Vibrational Solvation-Correlation Functions from Three-Pulse Infrared Photon Echoes. *J. Phys. Chem. B* **2002**, *106*, 8055−8063.
(63) Kwac, K.; Cho, M. Molecular Dynamics Simulation Study of N-Methylacetamide in Water. II. Two-Dimensional Infrared Pump-Probe Spectra. *J. Chem. Phys.* **2003**, *119*, 2256−2263.
(64) Eaves, J. D.; Loparo, J. J.; Fecko, C. J.; Roberts, S. T.; Tokmakoff, A.; Geissler, P. L. Hydrogen Bonds in Liquid Water are Broken Only Fleetingly. *Proc. Natl. Acad. Sci. U.S.A.* **2005**, *102*, 13019−13022.
(65) Loparo, J. J.; Roberts, S. T.; Tokmakoff, A. Multidimensional Infrared Spectroscopy of Water. II. Hydrogen Bond Switching Dynamics. *J. Chem. Phys.* **2006**, *125*, 194522−1−194522−12.
(66) Finkelstein, I. J.; Ishikawa, H.; Kim, S.; Massari, A. M.; Fayer, M. D. Substrate Binding and Protein Conformational Dynamics Measured by 2D-IR Vibrational Echo Spectroscopy. *Proc. Natl. Acad. Sci. U.S.A.* **2007**, *104*, 2637−2642.
(67) Fang, C.; Bauman, J. D.; Das, K.; Remorino, A.; Arnold, E.; Hochstrasser, R. M. Two-Dimensional Infrared Spectra Reveal Relaxation of the Nonnucleoside Inhibitor TMC278 Complexed with HIV-1 Reverse Transcriptase. *Proc. Natl. Acad. Sci. U.S.A.* **2008**, *105*, 1472−1477.
(68) Kraemer, D.; Cowan, M. L.; Paarmann, A.; Huse, N.; Nibbering, E. T. J.; Elsaesser, T.; Miller, R. J. D. Temperature Dependence of the Two-Dimensional Infrared Spectrum of Liquid H_2O. *Proc. Natl. Acad. Sci. U.S.A.* **2008**, *105*, 437−442.
(69) Asbury, J. B.; Steinel, T.; Kwak, K.; Corcelli, S. A.; Lawrence, C. P.; Skinner, J. L.; Fayer, M. D. Dynamics of Water Probed with Vibrational Echo Correlation Spectroscopy. *J. Chem. Phys.* **2004**, *121*, 12431−12446.
(70) Kwak, K.; Park, S.; Finkelstein, I. J.; Fayer, M. D. Frequency-Frequency Correlation Functions and Apodization in Two-Dimensional Infrared Vibrational Echo Spectroscopy: A New Approach. *J. Chem. Phys.* **2007**, *127*, 124503-1−124503-17.